1 **Method to measure the size-resolved real part of aerosol refractive index**

2 Gang Zhao[1], Weilun Zhao[1], Chunsheng Zhao[1*]

3 1 Department of Atmospheric and Oceanic Sciences, School of Physics, Peking University, Beijing,

4 China

5 *Correspondence to: Chunsheng Zhao (zcs@pku.edu.cn)*

6 **Abstract**

7 Knowledge on the refractive index of ambient aerosol can help reduce the uncertainties in

8 estimating aerosol radiative forcing. A new method is proposed to retrieve the size-resolved real part

9 of RI (RRI). Main principle of deriving the RRI is measuring the scattering intensity by single particle

10 soot photometer of size-selected aerosol. This method is validated by a series of calibration

11 experiments using the components of known RI. The retrieved size-resolved RRI cover a wide range

12 from 200nm to 450nm with uncertainty less than 0.02. Measurements of the size resolved real part of

13 the aerosol refractive index can improve the understanding of the aerosol radiative effects.

14 **1 Introduction**

15 Aerosols exert significant influence on the earth energy budget by scattering and absorbing

16 radiation (Ramanathan and Carmichael, 2008). There still remain great uncertainties when estimating

17 the aerosol effective radiative forcing (RF) (Ghan and Schwartz, 2007) and an accurate estimation of

18 the aerosol optical properties can help reduce the RF variations. The optical properties of the ambient

19 aerosol particles are determined by their particle size and complex refractive index (RI, m=n+ki)

20 (Bohren and Huffman, 2007;Levoni et al., 1997). Despite that the ambient aerosol particle size

21 distribution can be measured with high accuracy (Wiedensohler et al., 2012), an accurate measurement

22 of the ambient aerosol RI remains challenging. The RI is also widely used in remote sensing

23 (Redemann et al., 2000;Dubovik, 2002;Zhao et al., 2017) and atmospheric modelling (Ghan and

24 Schwartz, 2007;Kuang et al., 2015) because the aerosol single scattering albedo (SSA) and aerosol

25 scattering phase function are highly related with the RI. At the same time, a small uncertainty in the

26 real part of the RI (RRI) can lead to great uncertainties when estimating the aerosol RF. Zarzana et al.

27 (2014) finds that a variation of 0.003 in RRI can lead to uncertainties of 1% in RF for non-absorbing

28 ammonium sulfate particles. Moise et al. (2015) estimates that the RF will increase 12% when the RRI

29 varies from 1.4 to 1.5. Valenzuela et al. (2018) also reports an uncertainty of 7% with the uncertainties

30 of RRI of 0.1 in RRI. Therefore, it is pressing that the uncertainties of the RI be reduced when

31 estimating the RF.

32   Many methods were proposed to derive the RRI. The RRI can be estimated by linear volume

33 average of the known aerosol chemical components by

34 $$\mathrm{n} = \sum_i f_i n_i \qquad (1)$$

35 where f_i and n_i is the volume fraction and known partial refractive index of ith component (Wex et

36 al., 2002;Hand and Kreidenweis, 2002;Hanel, 1968;Liu and Daum, 2008). The aerosol RRI can also

37 be calculated by partial molar refraction approach (Stelson, 1990;Hu et al., 2012) which is essentially

38 consistent with the linear volume method (Liu and Daum, 2008). The ambient aerosol RRI can be

39 derived by synthetically using the radiative transfer calculations and the ground-based solar extinction

40 and scattering measurements (Wendisch and Hoyningen-Huene, 1994, 1992). Sorooshian et al. (2008)

41 developed a method to measure the aerosol RRI based on the differential mobility analyzer (DMA)

42 and an optical particle counters. The RRI is retrieved from the known particle size from the DMA and

43 the aerosol scattering intensity from the Optical Particle Counter (OPC) for aerosol particles larger

44 than 500nm. The Scanning Mobility Particle Sizer (SMPS) and OPC is used in combination to derive

45 the RRI by aligning the particle size distributions in the instrument overlap regions (Hand and

46 Kreidenweis, 2002;Vratolis et al., 2018). The aerosol effective RRI is also retrieved by applying Mie

47 scattering theory to the aerosol particle number size distribution, aerosol bulk scattering coefficient

48 and aerosol absorbing coefficient data (Cai et al., 2011;Liu and Daum, 2000). Spindler et al. (2007)

49 retrieved the aerosol RRI value by using the cavity ring-down spectroscopy to measuring the scattering

50 and absorbing properties of bulk aerosols. Eidhammer et al. (2008)) measured the light scattering at

51 different angles and retrieved the RRI. Similarly, the aerosol RRI is retrieved by measuring the aerosol

52 phase function (Barkey et al., 2007). Recently, a method by using the single particle mass spectrometry

53 is proposed to measure the aerosol RRI (Zhang et al., 2015). At the same time, aerosol time-of-flight

54 mass spectrometer is proved to be capable of measuring the aerosol RRI (Moffet et al., 2008). The

55 aerosol RRI can also be retrieved from the Mie spectroscopy by using the optical tweezers in the

56 laboratory (Shepherd et al., 2018).

57   Up to now, there is no information in the literature of the size-resolved ambient aerosol RRI over

58 the diameter range between 200nm and 500nm where the aerosol scattering coefficients contributes to

59 the total scattering coefficients most (Tao et al., 2017;Kuang et al., 2018). All the instruments

60 mentioned above can only measure the total equivalent aerosol RRI or aerosol RRI at a given diameter.

61 However, many studies show that aerosol of different diameter shares different properties such as

62 shape (Zhang et al., 2016;Peng et al., 2016), density (Qiao et al., 2018), aerosol hygroscopicity (Wang

63 et al., 2017) and most importantly, the chemical components (Liu et al., 2014;Hu et al., 2012). Thus,

64 there might be significant variations in the aerosol RRI for aerosols of different diameter because the

65 aerosol RRI is highly related to the aerosol density (Liu and Daum, 2008) and chemical components

66 (Stelson, 1990). On the other way round, information of the size-resolved aerosol RRI can help to

67 study the chemical information and the aging process of aerosols among different diameters. Therefore,

68 measurement of the size-resolved aerosol RRI is necessary.

69   In this study, a novel method is proposed to measure the size-resolved ambient aerosol RRI by

70 using a DMA in tandem with a single particle soot photometer (SP2). The principle of the system is

71 using the SP2 to measure the scattering properties of size-selected aerosols. Knowing the aerosol

72 diameter and corresponding scattering intensity, the size-resolved aerosol RRI can be retrieved based

73 on the Mie scattering theory. This proposed method can measure the ambient aerosol RRI over a wide

74 size range with high accuracy. The measurement system is employed in a field campaign in the North

75 China Plain and the corresponding results are further discussed.

76   The structure of this manuscript is as follows: section 2 provides the instruments setup and details

77 of the instrument. The method of retrieving the size-resolved aerosol RRI is given in section 3. Section

78 4 shows the discussions about the uncertainties of the proposed method and field measurements results

79 of the size-resolved aerosol RRI. Conclusions come at the last part.

80 **2 Instrument**

81 **2.1 Instrument Setup**

82   The instrument setup is schematically shown in fig. 1(a). Firstly, the dried sample aerosols are

83 guided to a X-ray soft diffusion charger and then lead to a DMA (Model 3081, TSI, USA). The quasi-

84 monodisperse aerosols that pass though the DMA at a given diameter are then drawn into a SP2 to

85 measure the aerosol scattering properties with a flow ratio of 0.12 lpm and a condensation particle

86 counter (CPC, Model 3776, TSI, USA) to count the aerosol number concentration with a flow ratio of

87 0.28 lpm respectively. Thus, the sample flow (Q_a) of the DMA is 0.4 lpm. Accordingly, the sheath

88 flow (Q_{sh}) of the DMA is 4 lpm. The DMA is set to scan the aerosols diameter from 12.3 to 697 nm

89   over a period of 285s and repeats after a pause of 15s. Thus, the combination of DMA, CPC and SP2

90   can provide the aerosol PNSD and size-resolved RRI every 5 minutes.

91   On 8th, June, 2018, the measurement system was employed at the filed measurement of

92   AERONET station of BEIJING_PKU (N39°59′, E116°18′) to test the reliability of retrieving the

93   ambient size-resolved RRI. This measurement site locates on the north west of the city of Beijing,

94   China and is about 1.8 km north of the Zhongguancun, Haidian District, which is one of the busiest

95   areas in Beijing. It is surrounded by two main streets: Zhongguancun North Street to the west and

96   Chengfu Road to the south. This site can provide representative information of the urban roadside

97   aerosols (Zhao et al., 2018).

98   **2.2 DMA**

99   When a voltage (V) is applied to the DMA, only a narrow size range of aerosol particles, with the

100   same electrical mobility (Z_p) can pass through the DMA (Knutson and Whitby, 1975). The Z_p is

101   expressed as:

$$Z_P = \frac{Q_{sh}}{2\pi V L} \ln\left(\frac{r_1}{r_2}\right) \qquad (2)$$

103   where Q_{sh} is the sheath flow rate; r_1 is the outer radius of annular space and r_2 is the inner radius of the

104   annular space. The transfer function refers to the probability that a particle with a certain electrical

105   mobility can pass through the DMA. For a given V, the transfer function is triangular-shaped, with the

106   peaking value of 100% and a half width (HW) of

$$\Delta Z_p = Z_P \frac{Q_a}{Q_{sh}} \qquad (3).$$

108   The aerosol Z_p, which is highly related to the aerosols diameter (D_p) and the number of elementary

109   charges on the particle (n), is defined as:

$$Z_p = \frac{neC(D_p)}{3\pi\mu D_p} \qquad (4)$$

111   where e is the elementary charge; μ is the gas viscosity coefficient, $C(D_p)$ is the Cunningham slip

112   correction that is defined by:

$$C = 1 + \frac{2\tau}{D_p}\left(1.142 + 0.558 e^{-\frac{0.999 D_p}{2\tau}}\right) \qquad (5)$$

114   where τ is the gas mean free path.

115   Based on the discussion above, the aerosols that pass through the DMA with the same Z_p, can have

116   different D_p and different elementary charges.

117   **2.3 SP2**

118   The SP2 is a widely used instrument that can measure the optical properties of every single particle.

119   The measurement principle and instrumental setup of the SP2 have been discussed in detail previously

120   (Stephens et al., 2003;Schwarz et al., 2006) and will be briefly described here. When the sample

121   aerosol particles pass through the continuous Nd:YAG laser beam at 1064nm with power about 1

122   mW/cm^2, eight sensors distributed at four directions are synchronously detecting the emitted or

123   scattered light by using avalanche photo-detector (APD) at different angles (45° and 135°). For each

124   direction, the two APDs sample the same signal with different sensitivities to get a wider measurement

125   range. The low gain channels are less sensitive to the measured signal and can be used to measure the

126   stronger signal of larger particles. In accordance, the high gain channels are more sensitive to the

127   measured signal, and can be used to measure the weaker signal of smaller particles. The optical head

128   of the SP2 is shown schematically in fig. 1(b).

129   In this study, we utilize signals from four channels of the SP2: two of them measure the scattering

130   signals and another two measure the incandescent light between 350 nm and 800 nm. The peak height

131   (H) of the incandescence signals is used to infer whether the sampled aerosol contains the black carbon

132   (BC). If the H of the incandescence signal is larger than 500, the sample aerosol contains the BC and

133   the scattering signals should deviate from the signals of pure scattering aerosol. Those sample aerosols

134   are ruled out when dealing with the aerosol scattering signals.

135   **3 Methodology**

136   **3.1 Scattering strength measured by the SP2**

137   From fig. 1(b), the APDs of the SP2 receive signals that were scattered by the sampled aerosols

138   from the directions at 45° and 135°. Thus, the scattering intensity (S) measured by the APD can be

139   expressed as:

140    $$S = C \cdot I_0 \cdot \sigma \cdot (PF_{45^o} + PF_{135^o}) \qquad (6),$$

141   where I_0 is the laser's intensity; σ is the scattering coefficient of the sampled aerosol, PF_{45^o} and

142   PF_{135^o} are scattering phase function at 45° and 135° respectively of the sampled aerosols; and C is

143   constant that is determined by the distance from the aerosol to the APD and the area of the APD. The

144   scattering intensity of the aerosol is recorded as the H of the scattering signals by SP2. Therefore, the

145   SP2 can be used as a powerful tool to measure the scattering signals of the sampled aerosol and the

146   influence of the BC on the aerosol scattering properties can be avoided. Based on the Mie scattering

147   theory, σ, PF_{45^o} and PF_{135^o} are determined by the size and RRI of the aerosol.

148   The amount of scattering signals from the sample aerosol varies with the diameter and RRI of the

149   aerosol (Bohren and Huffman, 2007). The scattering intensity at different aerosol diameter and RRI is

150   calculated based on equation (6) and shown in fig. 2. The C is assumed to be 1 here. From fig. 2, we

151   can see that the aerosol scattering intensity increases homogeneously with the increasing aerosol RRI

152   at a given Dp, which makes it possible to retrieve the aerosol RRI when the Dp and the scattering

153   intensity are known.

154   Bridging the scattering H values measured by the SP2 scattering channel and the scattering

155   intensity defined by equation 6 is achieved by calibrating the SP2 with ammonium sulfate. The

156   instrument setup of the calibration procedure is the same as that described in section 2.2.1. The

157   diameters of the aerosols passing through the DMA are manually changed from 100 to 450nm with a

158   step of 10nm. For each diameter, the scattering H value and incandescence signal of every particle are

159   analyzed. When calibrating, there is no aerosol whose incandescence signal exceeds 1000, which

160   means that the SP2 works stably and the incandescence signal channel can well distinguish the BC

161   containing aerosols.

162   After the calibration, the size-resolved RRI can be retrieved with known aerosol diameter selected

163   by DMA and the corresponding aerosol scattering H values measured by SP2.

164   **3.2 Multiple Charging**

165   Fig. S2 gives the aerosols scattering H probability distribution under different aerosol diameter.

166   For each diameter, the distributions of the scattering H may have more than one mode for both the high

167   gain and low gain channels. The following discussions would give explanation about the multiple

168   mode distributions of H.

169   For each mode, the number of recorded aerosol particles at a given H is fit by the log-normal

170   distribution function:

171    $$N(H) = \frac{N_0}{\sqrt{2\pi}\log(\sigma_g)} \cdot exp\left[-\frac{\log(H)-\log(H_0)}{2log^2(\sigma_g)}\right] \qquad (7)$$

172   Where σ_g is the geometric standard deviation; H_0 is the geometric standard mean H and N_0 is the

173   number concentrations for a peak mode. The geometric standard deviation is highly related to the half

174   width of the transfer function (equation 3) and the H_0 is discussed below in detail.

175   The H_0 values of each mode at different diameters are labeled with different markers in fig. 2. The

176   σ_g is fitted to be a small range at 1.182 ± 0.02 for different mode and different aerosol diameter. In

177   the following discussion, we conclude that the different PH_0 values in fig. 3 represent that the aerosols

178   are charged with different number of elementary charges. Based on the Mie scattering theory (Bohren

179   and Huffman, 2007), the scattering intensity increases with increasing Dp, which imply that the H_0

180   should increase with the increment of Dp. Thus, the black square markers in fig.2 represent the aerosols

181   that are singly charged. At the same time, the relationships between the H_0 and Dp can be interpolated.

182   Other colored markers represent that the aerosols have more than one charge. We calculated the

183   corresponding diameter of the aerosols that share the same Z_p but different charges at the given Dp by

184   the DMA ($\widetilde{Dp}$). Then the corresponding H_0 at $\widetilde{Dp}$ are calculated and shown in dashed line in fig.2.

185   From fig.2, the calculated H_0 shows good consistence with the measured H_0.

186   From the discussion above, we conclude that the SP2 detect those ammonium sulfate aerosols

187   with the diameter larger than 160nm. However, the ambient aerosol RRI is always lower than that of

188   ammonium sulfate (Liu and Daum, 2008), thus the lower detecting limit of the ambient scattering

189   aerosols should be larger than 160nm. The measured H_0 of the SP2 scattering low gain channel signals

190   are shown in fig. S2. From fig. S2, the same results can be deduced as those of the high gain channel

191   signals.

192   Fig. 4(a) gives the relationships between the calculated scattering intensity and the SP2 aerosol

193   scattering H at different diameter. When calculating the scattering intensity, the RRI value of

194   ammonium sulfate is set to be 1.521. We can see that the aerosol scattering intensity shows good

195   consistence with the peak height (R^2=0.9992).

196   Furthermore, the RRI of the scattering aerosol at a given diameter can be retrieved using the

197   corresponding scattering H.

198   **3.3 Validation of the calibration**

199   Ammonium chloride is used to validate the method of deriving the RRI from SP2. The RRI value

200   of ammonium chloride is 1.642. The scattering H of the ammonium chloride under different diameters

201   are measured and analyzed. Fig. 4(b) shows the comparison between the measured scattering high gain

202   peak height and the theoretical peak height at different aerosols diameter. Results show that the

203   measured peak height and the calculated ones are well correlated with R^2=0.9994, which means that

204   the DMA and SP2 can be used to derived the aerosol RRI with high accuracy.

205   Fig. S3 gives the corresponding results of the scattering low gain channel. In fig. S3, the

206   relationship between the aerosol scattering peak height of the low gain channel and the scattering

207   strength is determined. At the same time, the comparison between the measured peak height and the

208   calculated peak height shows good consistence too.

209   **4 Results and Discussion**

210   **4.1 Field Measurements**

211   Figure 5 shows the measured average probability distribution of the ambient size-resolved RRI

212   and the measured mean PNSD. From fig. 5, we can see that the derived RRI is 1.46 ± 0.02 and doesn't

213   vary significantly with diameter between 199 nm and 436 nm. The measured aerosol PNSD during the

214   measurement has a maximum of 26400 #/cm^3 at 107 nm. Based on the measured PNSD and the

215   measured RRI, the size distribution of the scattering coefficient is calculated based on the Mie

216   scattering theory. The results in fig. 5 show that the measured RRI diameter range covers most of the

217   aerosol that contributes significantly to the aerosol scattering properties. Thus, the derived size-

218   resolved RRI of this range is representative of the ambient aerosols scattering properties.

219   **4.2 Uncertainty analysis**

220   The factors that influence the accuracy of retrieving RRI include the aerosols scattering H

221   measured by SP and the aerosol diameter selected by DMA.

222   The uncertainties of the selected diameter by DMA is well characterized based on equation 2 and

223   3. The uncertainties from the DMA transfer function can be avoided by fitting the scattering H using

224   the log-normal distribution function. However, the uncertainties of the measured H from the SP2

225   remain unknown. The HW of the transfer function is 0.1 times the scanning diameter, which means

226   that the geometric standard deviation of the aerosol PNSD selected by the DMA is estimated to be

227   1.102. At the same time, the measured geometric standard deviation of the measured H mode by SP2

228   is 1.182. Thus, the geometric standard deviation of the measured H from the SP2 is estimated to be

229   1.073, whose corresponding uncertainties is 6.8%.

230   The uncertainties of the retrieved RRI to the variations in the measured H are analyzed using the

231   Mie scattering theory and the corresponding results are shown in fig. 6. The variations in RRI increase

232   with the increment of RRI but decrease with the increment of the Dp. For most ambient aerosols, the

233   RRI ranges from 1.4 to 1.5 and corresponds to a variation in RRI of 0.015.

234   Table 1 lists the retrieved ammonium chloride RRI under different diameter. The absolute

235   difference between the retrieved RRI and theoretical values is always smaller than 0.02 regardless of

236   the particle diameter, which means that the measured RRI is in line with the theoretical one. Thus, we

237   conclude that the uncertainty of the retrieved RRI is within 0.02.

238   **5 Conclusions**

239   Knowledge on the microphysical properties of ambient aerosol is import for better evaluating

240   their radiative forcing. The aerosol RRI is a key factor that determines the aerosol scattering properties.

241   In this study, a new method to measure the ambient aerosol RRI is developed by synthetically using a

242   DMA in tandem with a SP2. This method can continuously measure the size-resolved RRI over a wide

243   range between 198 nm and 426 nm with an accuracy of 0.02. At the same time, it is free from the

244   influence of the BC containing aerosols.

245   The basic principle of measuring the size-resolved RRI is to select the aerosols at a certain

246   diameter by the DMA and measure the corresponding scattering intensity by the SP2. The relationship

247   between the aerosols scattering intensity and the peak height of the scattering signal channels are

248   determined by calibrating the SP2 using ammonium sulfate (RRI=1.521).

249   The method is validated by using the ammonium chloride with the RRI of 1.642 as sample aerosol

250   and the corresponding derived size-resolved RRI is 1.642 ± 0.02.

251   This instrument is employed at a field measurement at the AERONET PKU stating, the size-

252   resolved RRI of the ambient aerosols is 1.46 and doesn't show significant variation among the diameter.

253   The corresponding aerosol diameter range, which can be detected by SP2 to derive the RRI, covers

254   most of the aerosol scattering. Thus, the derived size-resolved RRI of this range can be used as a good

255   representative of the ambient aerosols scattering properties.

256

257   *Data availability.* The measurement data involved in this study are available upon request to the

258   authors.

259

Author contributions. Gang Zhao and Chunsheng Zhao designed the experiments; Gang Zhao and Weilun Zhao conducted the measurements; Chunsheng Zhao and Gang Zhao discussed the results and wrote the manuscript.

Competing interests. The authors declare that they have no conflict of interest.

Acknowledgments. This work is supported by the National Key R&D Programa of China (2016YFC020000:Task 5) and the National Natural Science Foundation of China (41590872).

Barkey, B., Paulson, S. E., and Chung, A.: Genetic Algorithm Inversion of Dual Polarization Polar Nephelometer Data to Determine Aerosol Refractive Index, Aerosol Sci. Technol., 41, 751-760, 10.1080/02786820701432640, 2007.

Bohren, C. F., and Huffman, D. R.: Absorption and Scattering by a Sphere, in: Absorption and Scattering of Light by Small Particles, Wiley-VCH Verlag GmbH, 82-129, 2007.

Cai, Y., Montague, D. C., and Deshler, T.: Comparison of measured and calculated scattering from surface aerosols with an average, a size-dependent, and a time-dependent refractive index, Journal of Geophysical Research, 116, 10.1029/2010jd014607, 2011.

Dick, W. D., Ziemann, P. J., and McMurry, P. H.: Multiangle Light-Scattering Measurements of Refractive Index of Submicron Atmospheric Particles, Aerosol Sci. Technol., 41, 549-569, 10.1080/02786820701272012, 2007.

Dubovik, O.: Variability of absorption and optical properties of key aerosol types observed in worldwide locations, J.atmos.sci, 59, 590-608, 2002.

Eidhammer, T., Montague, D. C., and Deshler, T.: Determination of index of refraction and size of supermicrometer particles from light scattering measurements at two angles, Journal of Geophysical Research, 113, 10.1029/2007jd009607, 2008.

Ghan, S. J., and Schwartz, S. E.: Aerosol Properties and Processes: A Path from Field and Laboratory Measurements to Global Climate Models, Bulletin of the American Meteorological Society, 88, 1059-1084, 10.1175/bams-88-7-1059, 2007.

Hand, J. L., and Kreidenweis, S. M.: A New Method for Retrieving Particle Refractive Index and Effective Density from Aerosol Size Distribution Data, Aerosol Sci. Technol., 36, 1012-1026, 10.1080/02786820290092276, 2002.

Hanel, G.: REAL PART OF MEAN COMPLEX REFRACTIVE INDEX AND MEAN DENSITY OF SAMPLES OF ATMOSPHERIC AEROSOL PARTICLES, Tellus, 20, 371-&, 10.3402/tellusa.v20i3.10016, 1968.

Hu, M., Peng, J., Sun, K., Yue, D., Guo, S., Wiedensohler, A., and Wu, Z.: Estimation of size-resolved ambient particle density based on the measurement of aerosol number, mass, and chemical size distributions in the winter in Beijing, Environ Sci Technol, 46, 9941-9947, 10.1021/es204073t, 2012.

Knutson, E. O., and Whitby, K. T.: Aerosol classification by electric mobility: apparatus, theory, and

applications, Journal of Aerosol Science, 6, 443-451, https://doi.org/10.1016/0021-8502(75)90060-9, 1975.

Kuang, Y., Zhao, C. S., Tao, J. C., and Ma, N.: Diurnal variations of aerosol optical properties in the North China Plain and their influences on the estimates of direct aerosol radiative effect, Atmos. Chem. Phys., 15, 5761-5772, 10.5194/acp-15-5761-2015, 2015.

Kuang, Y., Zhao, C. S., Zhao, G., Tao, J. C., Xu, W., Ma, N., and Bian, Y. X.: A novel method for calculating ambient aerosol liquid water content based on measurements of a humidified nephelometer system, Atmospheric Measurement Techniques, 11, 2967-2982, 10.5194/amt-11-2967-2018, 2018.

Levoni, C., Cervino, M., Guzzi, R., and Torricella, F.: Atmospheric aerosol optical properties: a database of radiative characteristics for different components and classes, Appl Opt, 36, 8031-8041, 1997.

Liu, H. J., Zhao, C. S., Nekat, B., Ma, N., Wiedensohler, A., van Pinxteren, D., Spindler, G., Müller, K., and Herrmann, H.: Aerosol hygroscopicity derived from size-segregated chemical composition and its parameterization in the North China Plain, Atmospheric Chemistry and Physics, 14, 2525-2539, 10.5194/acp-14-2525-2014, 2014.

Liu, Y., and Daum, P. H.: THE EFFECT OF REFRACTIVE INDEX ON SIZE DISTRIBUTIONS AND LIGHT SCATTERING COEFFICIENTS DERIVED FROM OPTICAL PARTICLE COUNTERS ☆, Journal of Aerosol Science, 31, 945-957, 2000.

Liu, Y., and Daum, P. H.: Relationship of refractive index to mass density and self-consistency of mixing rules for multicomponent mixtures like ambient aerosols, Journal of Aerosol Science, 39, 974-986, 10.1016/j.jaerosci.2008.06.006, 2008.

Moffet, R. C., Qin, X., Rebotier, T., Furutani, H., and Prather, K. A.: Chemically segregated optical and microphysical properties of ambient aerosols measured in a single-particle mass spectrometer, Journal of Geophysical Research, 113, 10.1029/2007jd009393, 2008.

Moise, T., Flores, J. M., and Rudich, Y.: Optical properties of secondary organic aerosols and their changes by chemical processes, Chemical Reviews, 115, 4400-4439, 2015.

Peng, J., Hu, M., Guo, S., Du, Z., Zheng, J., Shang, D., Levy Zamora, M., Zeng, L., Shao, M., Wu, Y.-S., Zheng, J., Wang, Y., Glen, C. R., Collins, D. R., Molina, M. J., and Zhang, R.: Markedly enhanced absorption and direct radiative forcing of black carbon under polluted urban environments, Proceedings of the National Academy of Sciences, 113, 4266-4271, 10.1073/pnas.1602310113, 2016.

Qiao, K., Wu, Z., Pei, X., Liu, Q., Shang, D., Zheng, J., Du, Z., Zhu, W., Wu, Y., Lou, S., Guo, S., Chan, C. K., Pathak, R. K., Hallquist, M., and Hu, M.: Size-resolved effective density of submicron particles during summertime in the rural atmosphere of Beijing, China, Journal of Environmental Sciences, 10.1016/j.jes.2018.01.012, 2018.

Ramanathan, V., and Carmichael, G.: Global and regional climate changes due to black carbon, Nature Geoscience, 1, 221-227, 10.1038/ngeo156, 2008.

Redemann, J., Turco, R. P., Liou, K. N., Russell, P. B., Bergstrom, R. W., Schmid, B., Livingston, J. M., Hobbs, P. V., Hartley, W. S., Ismail, S., Ferrare, R. A., and Browell, E. V.: Retrieving the vertical structure of the effective aerosol complex index of refraction from a combination of aerosol in situ and remote sensing measurements during TARFOX, Journal of Geophysical Research: Atmospheres, 105, 9949-9970, 10.1029/1999jd901044, 2000.

Schwarz, J. P., Gao, R. S., Fahey, D. W., Thomson, D. S., Watts, L. A., Wilson, J. C., Reeves, J. M., Darbeheshti, M., Baumgardner, D. G., Kok, G. L., Chung, S. H., Schulz, M., Hendricks, J., Lauer, A.,

342 Kärcher, B., Slowik, J. G., Rosenlof, K. H., Thompson, T. L., Langford, A. O., Loewenstein, M., and
343 Aikin, K. C.: Single-particle measurements of midlatitude black carbon and light-scattering aerosols
344 from the boundary layer to the lower stratosphere, Journal of Geophysical Research, 111,
345 10.1029/2006jd007076, 2006.
346 Shepherd, R. H., King, M. D., Marks, A. A., Brough, N., and Ward, A. D.: Determination of the
347 refractive index of insoluble organic extracts from atmospheric aerosol over the visible
348 wavelength range using optical tweezers, Atmospheric Chemistry and Physics, 18, 5235-5252,
349 10.5194/acp-18-5235-2018, 2018.
350 Sorooshian, A., Hersey, S., Brechtel, F. J., Corless, A., Flagan, R. C., and Seinfeld, J. H.: Rapid, Size-
351 Resolved Aerosol Hygroscopic Growth Measurements: Differential Aerosol Sizing and
352 Hygroscopicity Spectrometer Probe (DASH-SP), Aerosol Sci. Technol., 42, 445-464,
353 10.1080/02786820802178506, 2008.
354 Spindler, C., Riziq, A. A., and Rudich, Y.: Retrieval of Aerosol Complex Refractive Index by
355 Combining Cavity Ring Down Aerosol Spectrometer Measurements with Full Size Distribution
356 Information, Aerosol Sci. Technol., 41, 1011-1017, 10.1080/02786820701682087, 2007.
357 Stelson, A. W.: Urban aerosol refractive index prediction by partial molar refraction approach,
358 Environ.sci.technol, 24:11, 1676-1679, 1990.
359 Stephens, M., Turner, N., and Sandberg, J.: Particle identification by laser-induced incandescence in a
360 solid-state laser cavity, Appl Opt, 42, 3726-3736, 2003.
361 Tao, J., Zhao, C., Kuang, Y., Zhao, G., Shen, C., Yu, Y., Bian, Y., and Xu, W.: A New Method for
362 Calculating Number Concentrations of Cloud Condensation Nulcei Based on Measurements of A
363 Three-wavelength Humidified Nephelometer System, Atmospheric Measurement Techniques
364 Discussions, 1-19, 10.5194/amt-2017-193, 2017.
365 Valenzuela, A., Reid, J. P., Bzdek, B. R., and Orr-Ewing, A. J.: Accuracy required in measurements of
366 refractive index and hygroscopic response to reduce uncertainties in estimates of aerosol radiative
367 forcing efficiency, Journal of Geophysical Research: Atmospheres, 10.1029/2018jd028365, 2018.
368 Vratolis, S., Fetfatzis, P., Argyrouli, A., Papayannis, A., Müller, D., Veselovskii, I., Bougiatioti, A.,
369 Nenes, A., Remoundaki, E., Diapouli, E., Manousakas, M., Mylonaki, M., and Eleftheriadis, K.: A
370 new method to retrieve the real part of the equivalent refractive index of atmospheric aerosols, Journal
371 of Aerosol Science, 117, 54-62, 10.1016/j.jaerosci.2017.12.013, 2018.
372 Wang, Y., Wu, Z., Ma, N., Wu, Y., Zeng, L., Zhao, C., and Wiedensohler, A.: Statistical analysis and
373 parameterization of the hygroscopic growth of the sub-micrometer urban background aerosol in
374 Beijing, Atmospheric Environment, 10.1016/j.atmosenv.2017.12.003, 2017.
375 Wendisch, M., and Hoyningen-Huene, W. V.: Optically equivalent refractive index of atmospheric
376 aerosol particles, Huene, 65, 1992.
377 Wendisch, M., and Hoyningen-Huene, W. V.: Possibility of refractive index determination of
378 atmospheric aerosol particles by ground-based solar extinction and scattering measurements,
379 Atmospheric Environment, 28, 785-792, 1994.
380 Wex, H., Neusüß, C., Wendisch, M., Stratmann, F., Koziar, C., Keil, A., Wiedensohler, A., and Ebert,
381 M.: Particle scattering, backscattering, and absorption coefficients: An in situ closure and sensitivity
382 study, Journal of Geophysical Research: Atmospheres, 107, LAC 4-1-LAC 4-18,
383 10.1029/2000jd000234, 2002.
384 Wiedensohler, A., Birmili, W., Nowak, A., Sonntag, A., Weinhold, K., Merkel, M., Wehner, B., Tuch,
385 T., Pfeifer, S., Fiebig, M., Fjäraa, A. M., Asmi, E., Sellegri, K., Depuy, R., Venzac, H., Villani, P., Laj,

386 P., Aalto, P., Ogren, J. A., Swietlicki, E., Williams, P., Roldin, P., Quincey, P., Hüglin, C., Fierz-
387 Schmidhauser, R., Gysel, M., Weingartner, E., Riccobono, F., Santos, S., Grüning, C., Faloon, K.,
388 Beddows, D., Harrison, R., Monahan, C., Jennings, S. G., O'Dowd, C. D., Marinoni, A., Horn, H. G.,
389 Keck, L., Jiang, J., Scheckman, J., McMurry, P. H., Deng, Z., Zhao, C. S., Moerman, M., Henzing, B.,
390 de Leeuw, G., Löschau, G., and Bastian, S.: Mobility particle size spectrometers: harmonization of
391 technical standards and data structure to facilitate high quality long-term observations of atmospheric
392 particle number size distributions, Atmospheric Measurement Techniques, 5, 657-685, 10.5194/amt-
393 5-657-2012, 2012.
394 Zarzana, K. J., Cappa, C. D., and Tolbert, M. A.: Sensitivity of Aerosol Refractive Index Retrievals
395 Using Optical Spectroscopy, Aerosol Sci. Technol., 48, 1133-1144, 10.1080/02786826.2014.963498,
396 2014.
397 Zhang, G., Bi, X., Han, B., Qiu, N., Dai, S., Wang, X., Sheng, G., and Fu, J.: Measurement of aerosol
398 effective density by single particle mass spectrometry, Science China Earth Sciences, 59, 320-327,
399 10.1007/s11430-015-5146-y, 2015.
400 Zhang, Y., Zhang, Q., Cheng, Y., Su, H., Kecorius, S., Wang, Z., Wu, Z., Hu, M., Zhu, T., Wiedensohler,
401 A., and He, K.: Measuring the morphology and density of internally mixed black carbon with SP2 and
402 VTDMA: new insight into the absorption enhancement of black carbon in the atmosphere,
403 Atmospheric Measurement Techniques, 9, 1833-1843, 10.5194/amt-9-1833-2016, 2016.
404 Zhao, G., Zhao, C., Kuang, Y., Tao, J., Tan, W., Bian, Y., Li, J., and Li, C.: Impact of aerosol
405 hygroscopic growth on retrieving aerosol extinction coefficient profiles from elastic-backscatter lidar
406 signals, Atmospheric Chemistry and Physics, 17, 12133-12143, 10.5194/acp-17-12133-2017, 2017.
407 Zhao, G., Zhao, C., Kuang, Y., Bian, Y., Tao, J., Shen, C., and Yu, Y.: Calculating the aerosol
408 asymmetry factor based on measurements from the humidified nephelometer system, Atmospheric
409 Chemistry and Physics, 18, 9049-9060, 10.5194/acp-18-9049-2018, 2018.

410

411

412
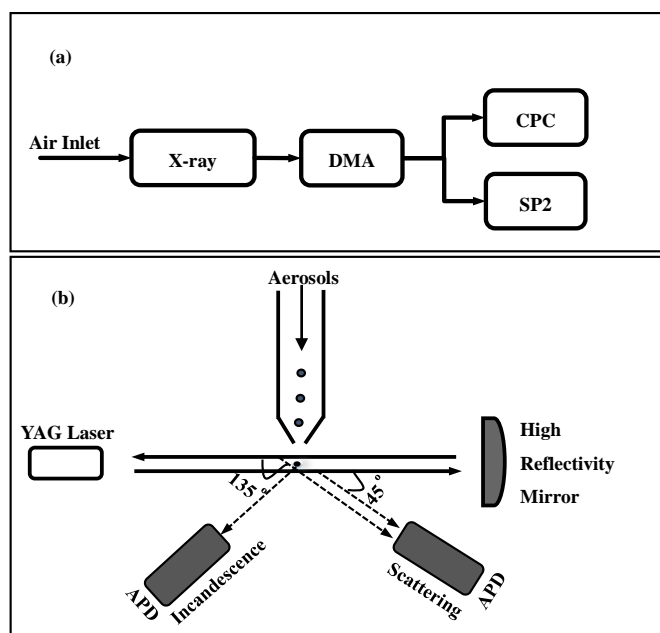
413   **Figure 1.** (a) Schematic of the measurement system. (b) Diagram of SP2 Chamber.

414
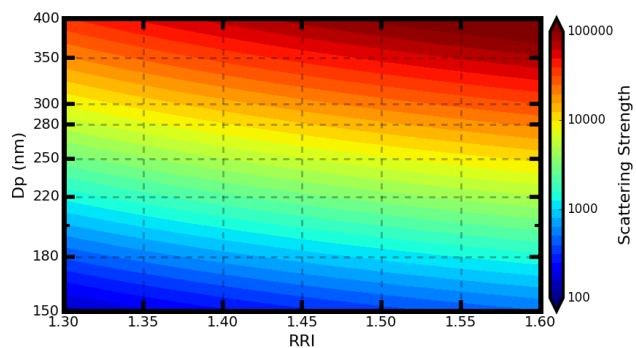
415   **Figure 2.** The distribution of the aerosols scattering strength at different Dp and different RRI.

416

417
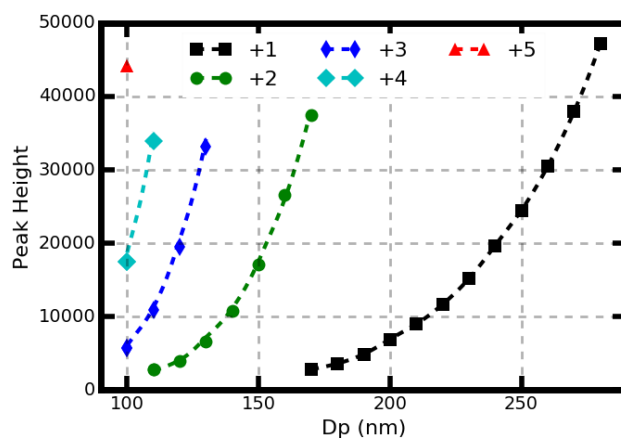
418 **Figure 3.** The geometric mean peak height for different diameters of the high gain. The markers gives

419 the measured values and the dotted line shows the theoretically calculated value. Different colors

420 represent the different number of elementary charges.

421
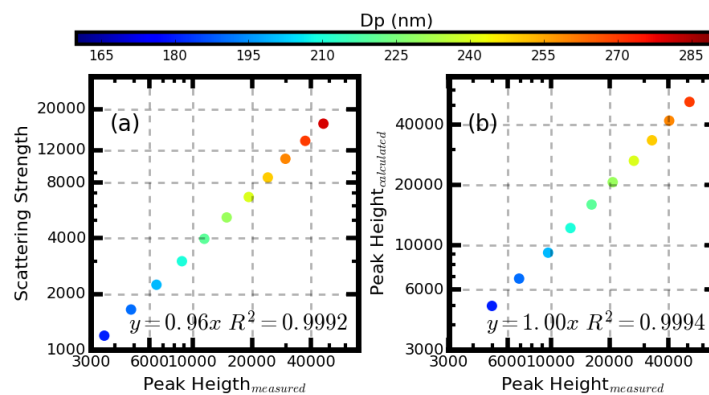
Figure 4. (a) the relationship between the scattering peak height from the SP2 high gain scattering channel using the ammonia sulfate and (b) the comparison between the measured scattering peak height from SP2 high gain scattering channel using the ammonia chloride and the calculated scattering peak height using the Mie scattering theory. Different colors represents the results at different diameter.

427
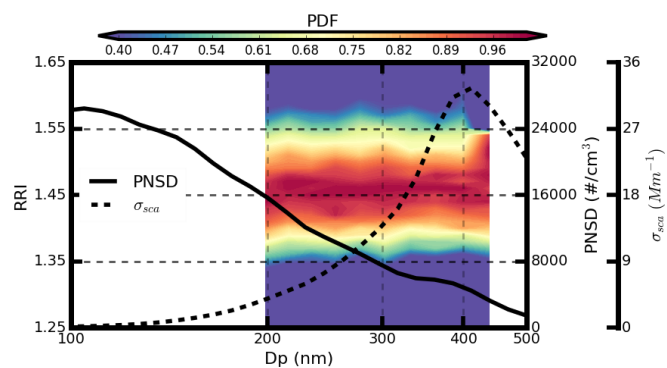
Figure 5. The measured probability of the size-resolved RRI (the filled color), the measured mean

PNSD (the full line) and the mean scattering size distribution (the dotted line).

430
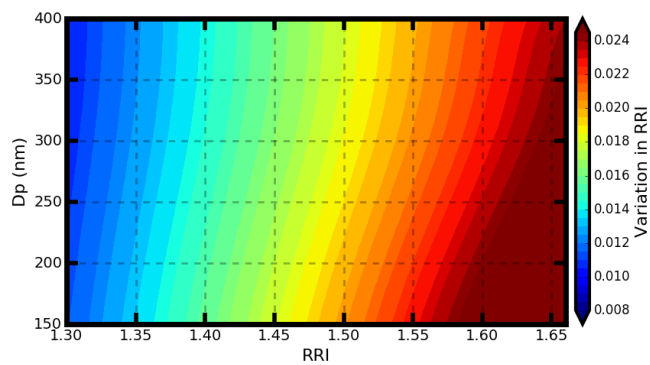
431   **Figure 6.** The variation in RRI for different kinds of aerosols that have different diameters and different

432   RRI.

433

434

435 **Tabel 1.** The retrieved RRI and the absolute difference between the retrieved RRI and the theoretical

436 RRI for different ammonia chloride diameter.

Dp(nm)	160	170	180	190	200	210	220	230	240	250	260	270
RRI	1.654	1.650	1.651	1.643	1.656	1.645	1.633	1.626	1.634	1.626	1.624	1.625
Difference	0.012	0.008	0.009	0.001	0.012	0.003	0.009	0.016	0.008	0.016	0.018	0.017

437